Supplementary Online Materials for:

Speleothem evidence for late Miocene extreme Arctic amplification - an analogue for near future anthropogenic climate change?

Stuart Umbo[1], Franziska Lechleitner[2], Thomas Opel[3], Sevasti Modestou[1], Tobias Braun[4,5], Anton Vaks[6], Gideon Henderson[7], Pete Scott[8], Alexander Osintzev[9], Alexandr Kononov[10,11], Irina Adrian[12], Yuri Dublyansky[13], Alena Giesche[14, 15], Sebastian F.M. Breitenbach[1]

[1]Department of Geography and Environmental Sciences, Northumbria University, Newcastle-upon-Tyne, NE1 8ST, United Kingdom
[2]Department of Chemistry, Biochemistry and Pharmaceutical Sciences & Oeschger Centre for Climate Change Research, Bern, 2012, Switzerland
[3]Alfred Wegener Institute Helmholtz Centre for Polar and Marine Research, Telegrafenberg A45, Potsdam, 14473, Germany
[4]Remote Sensing Centre for Earth System Research, Leipzig University, 04103, Leipzig, Germany
[5]Potsdam Institute for Climate Impact Research (PIK), Member of the Leibniz Association, 14473, Potsdam, Germany
[6]Geochemistry and Environmental Geology Division, Geological Survey of Israel, Jerusalem, 9692100, Israel
[7]Department of Earth Sciences, Oxford University, Oxford, OX1 3AN United Kingdom
[8]Oceans Institute, University of Western Australia, Perth, 6009, Australia
[9]Speleoclub Arabika, Irkutsk, 664058, Russian Federation
[10]Irkutsk Nation al Research Technical University, Irkutsk, 664074, Russia
[11]Institute of the Earth's Crust, Russian Academy of Sciences, Siberian Branch, Irkutsk, 664033, Russia
[12]Lena Delta Wildlife Reserve, Tiksi, Sakha Republic, 678400 Russia
[13]Institute of Geology, University of Innsbruck, Innrain 52, 6020, Innsbruck, Austria
[14]U.S. Geological Survey, Alaska Science Center, Anchorage, Alaska 99508, USA
[15]Department of Earth Sciences, Cambridge University, Cambridge CB2 3EQ, United Kingdom

Correspondence to: Stuart Umbo (stuart.umbo@northumbria.ac.uk)

Discussion of uncertainty in fluid inclusion and clumped isotope derived temperature estimates

We identify several sources of uncertainty in our fluid inclusion temperature estimate (T_{FI}). T_{FI} relies on the assumption that temperature is the sole driver of the calcite $\delta^{18}O$ signal and that $\delta^{18}O_{dw}$ remained constant (-17.5 ‰ VSMOW – obtained from our fluid inclusion measurement) along the entire STBB I – 1 record. Both assumptions rarely hold true in natural environments, with $\delta^{18}O$ fractionation also dependent on speleothem growth rate (Gabitov et al., 2012) and $\delta^{18}O$ of dripwater, itself largely controlled by hydroclimate conditions. In addition, the application of fluid inclusion temperature calibrations assumes negligible isotopic exchange between calcite and inclusion waters after the closure of the fluid inclusion. Such post-depositional exchange with host calcite has traditionally been ruled out by demonstrating that fluid inclusion water falls on the global meteoric water line (Meckler et al., 2021), as is the case in STBB I – 1 (Fig. S2). However, this observation assumes that the local meteoric water line remained constant since the Tortonian, which is unlikely. Even if post depositional isotopic exchange is present in STBB I - 1, recent laboratory experiments have suggested temperature offsets are minimal. Uemura et al. (2020) estimate temperature biases of ca. 0.5°C for a 10°C climate shift, and thus it seems an unlikely cause of major uncertainty in T_{FI}.

Several studies have demonstrated the tendency for speleothem clumped isotope temperatures to give unrealistically high temperatures as a result of isotopic disequilibrium caused by CO_2 degassing and depletion of the dissolved inorganic carbon (DIC) pool (Affek et al., 2008; Daëron et al., 2011). Kluge & Affek (2012) suggested that kinetic fractionation effects can lead to temperature offsets up to +10°C in speleothems from Bunker Cave in Germany. Yet, isotopic equilibrium is achieved in slow-growing subaqueous speleothems (Daëron et al., 2011) and where the DIC reservoir experiences constant replenishment. This is supported by the $\Delta 47$ calibration of Kele et al. (2015), which is based on travertines that experienced limited CO_2 degassing and DIC-speciation effects (Tripati et al., 2015).

Covariation of $\delta^{18}O$ and $\delta^{13}C$ along the speleothem can be utilised as an indicator of kinetic isotope fractionation as CO_2 degassing drives isotopic enrichment in the DIC pool through Rayleigh fractionation. A strong $\delta^{18}O$ vs $\delta^{13}C$ correlation is exhibited in STBB I - 1 ($r = 0.75$, $p < 0.0001$), and moderate correlation in STBB II - 7 ($r = 0.55$, $p < 0.0001$). We note that common environmental drivers can also cause covariation but stress that we cannot rule out some degree of kinetic isotope fractionation in our samples. However, agreement between our clumped isotope and fluid inclusion-based reconstructions, whilst not proof of equilibrium conditions, do suggest limited fractionation effects in our samples. Nevertheless, since isotopic disequilibrium tends to favour higher temperatures, we restrict our discussion of reconstructed Tortonian temperatures on the cooler $T_{\Delta 47}$ estimates derived from our in-house calibration.
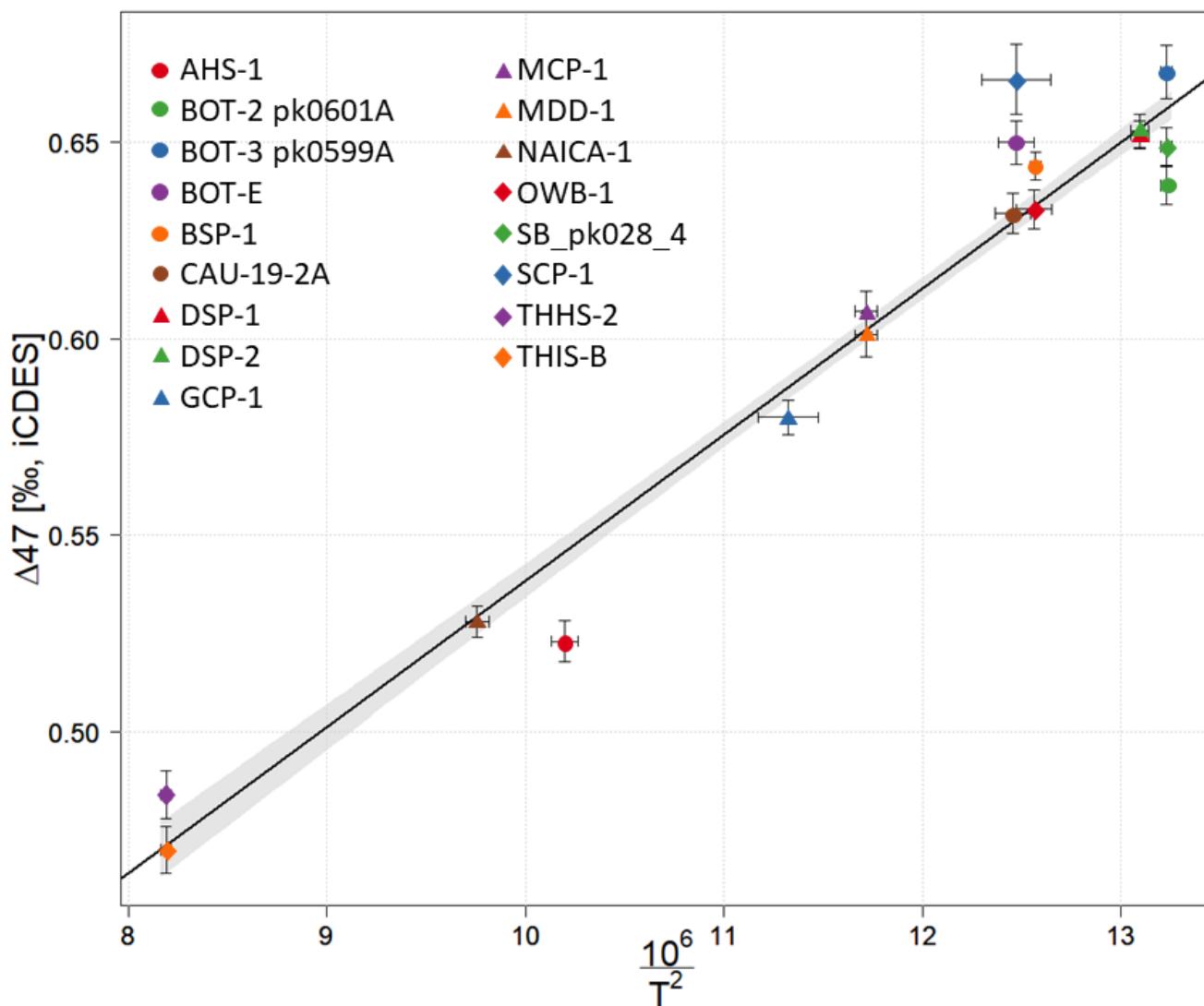
Figure S1: Northumbria University clumped isotope temperature calibration derived from 17 inorganic calcites precipitated at known temperatures. T is the known precipitation temperature in kelvin. Error bars are standard errors. The regression line is derived using a York least squares method (York et al., 2004) to account for uncertainty in both the X and Y dimensions. Grey shaded area is the 95% confidence interval.
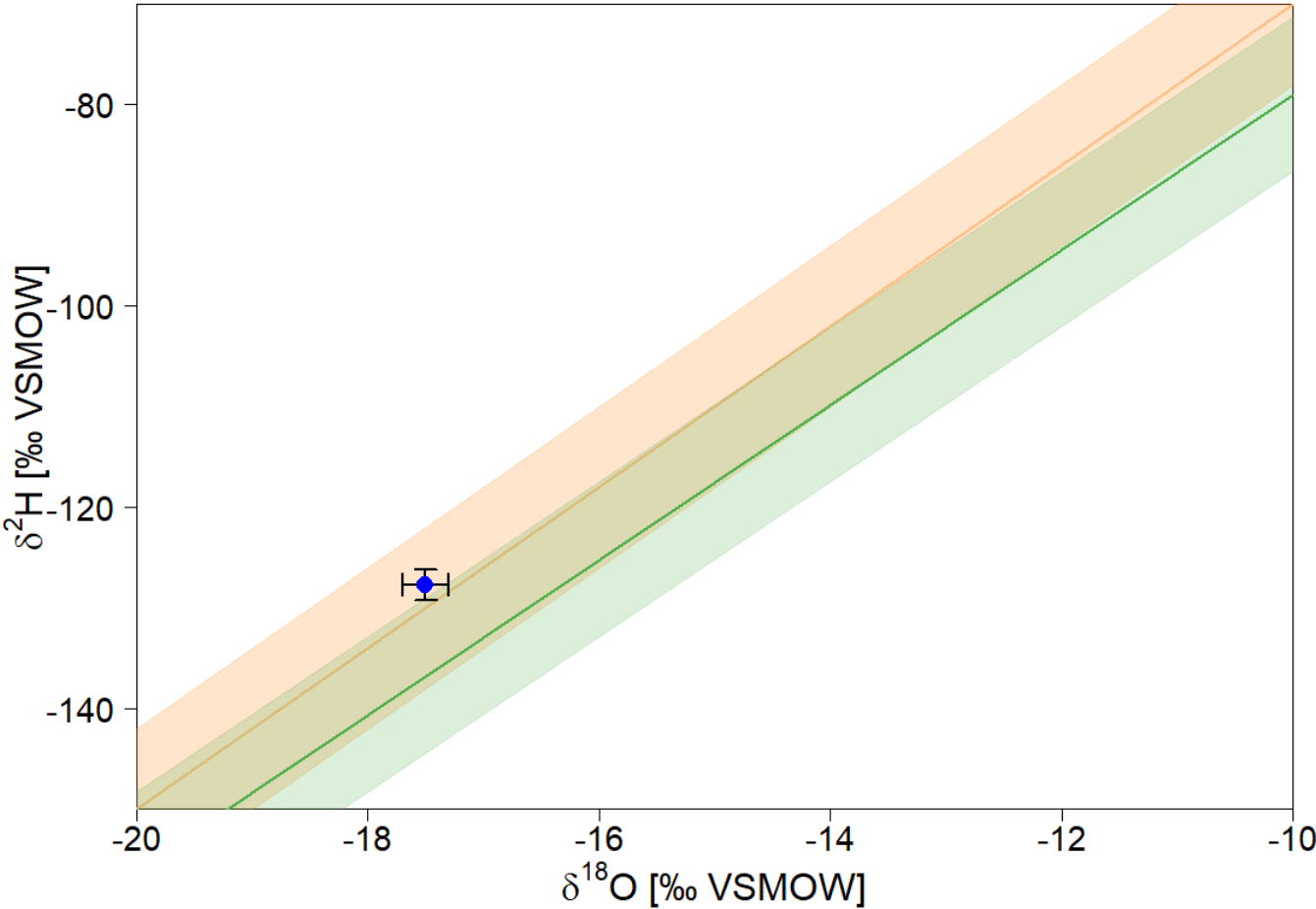
Figure S2: Fluid inclusion δ²H vs δ¹⁸O for sample STBB I – 1 (blue dot), compared with the Global Meteoric Water Line (orange)
 (Craig, 1961) and Local Meteoric Water Line (green), calculated from monthly mean precipitation data at the Samoylov Island Research Station (Spors, 2018). Shaded areas are ± 1 ‰ δ¹⁸O. Error bars are the measurement uncertainty.
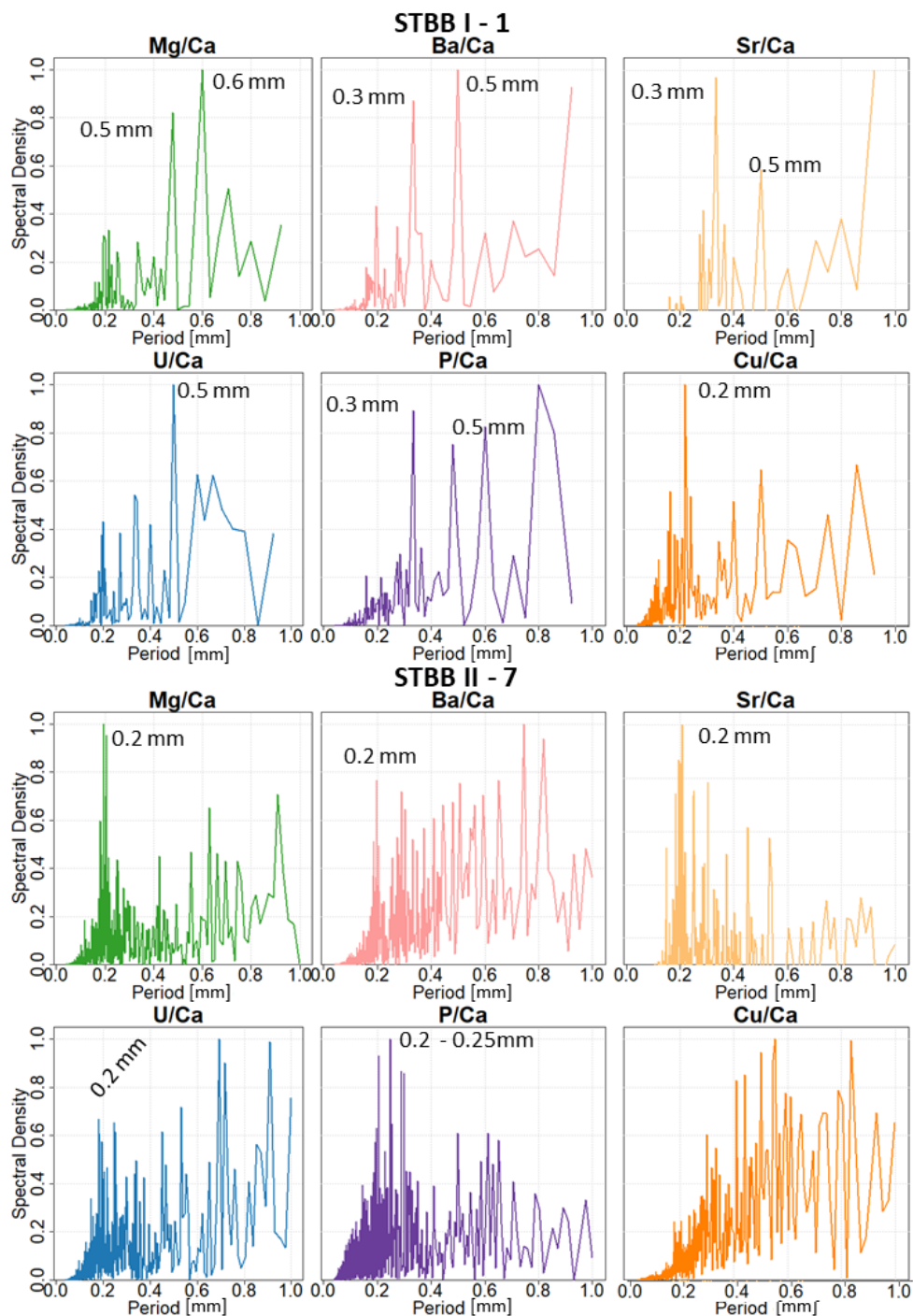
Figure S6~~3~~: Trace element spectral analysis results for STBB I – 1 and STBB II – 7. Dominant frequencies are noted next to peaks. STBB I - 1 exhibits common frequencies of ca. 0.3 and 0.5 mm in multiple proxies. STBB II - 7 exhibits regular cycles in all hydrological proxies at ca. 0.2 mm.

90
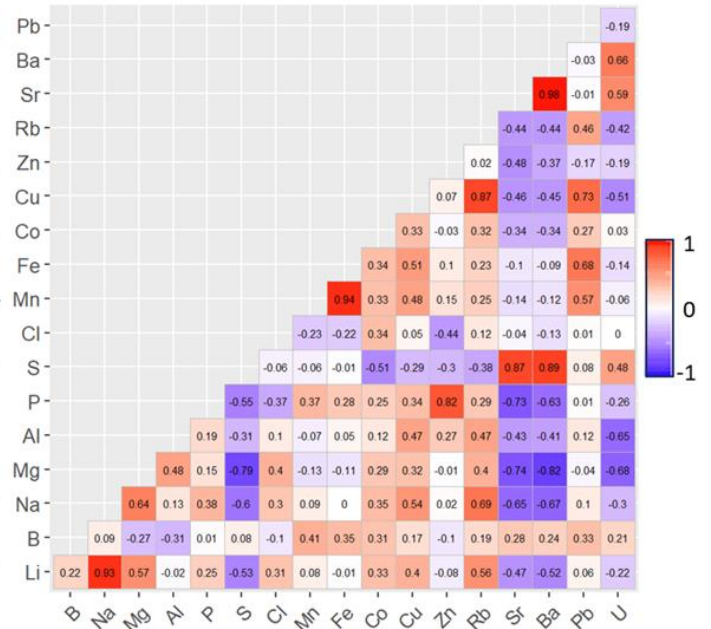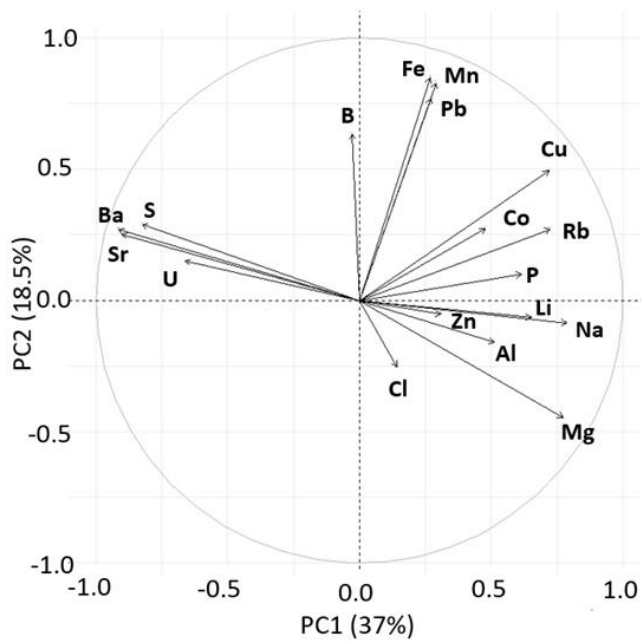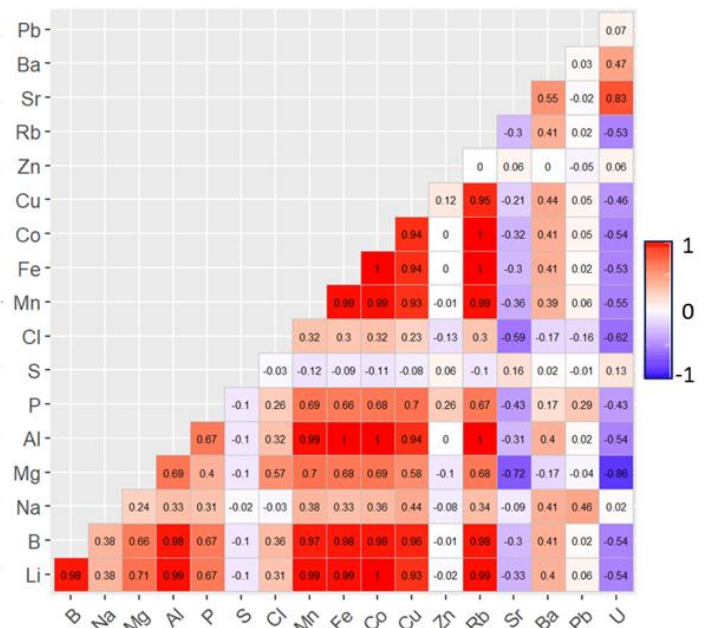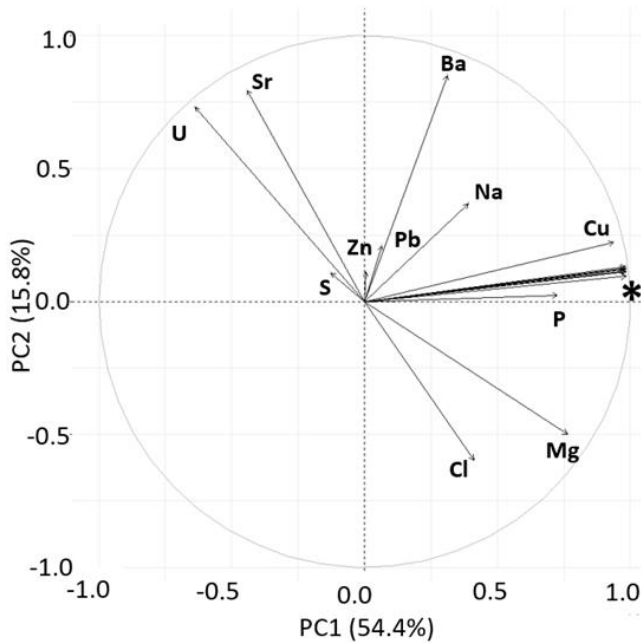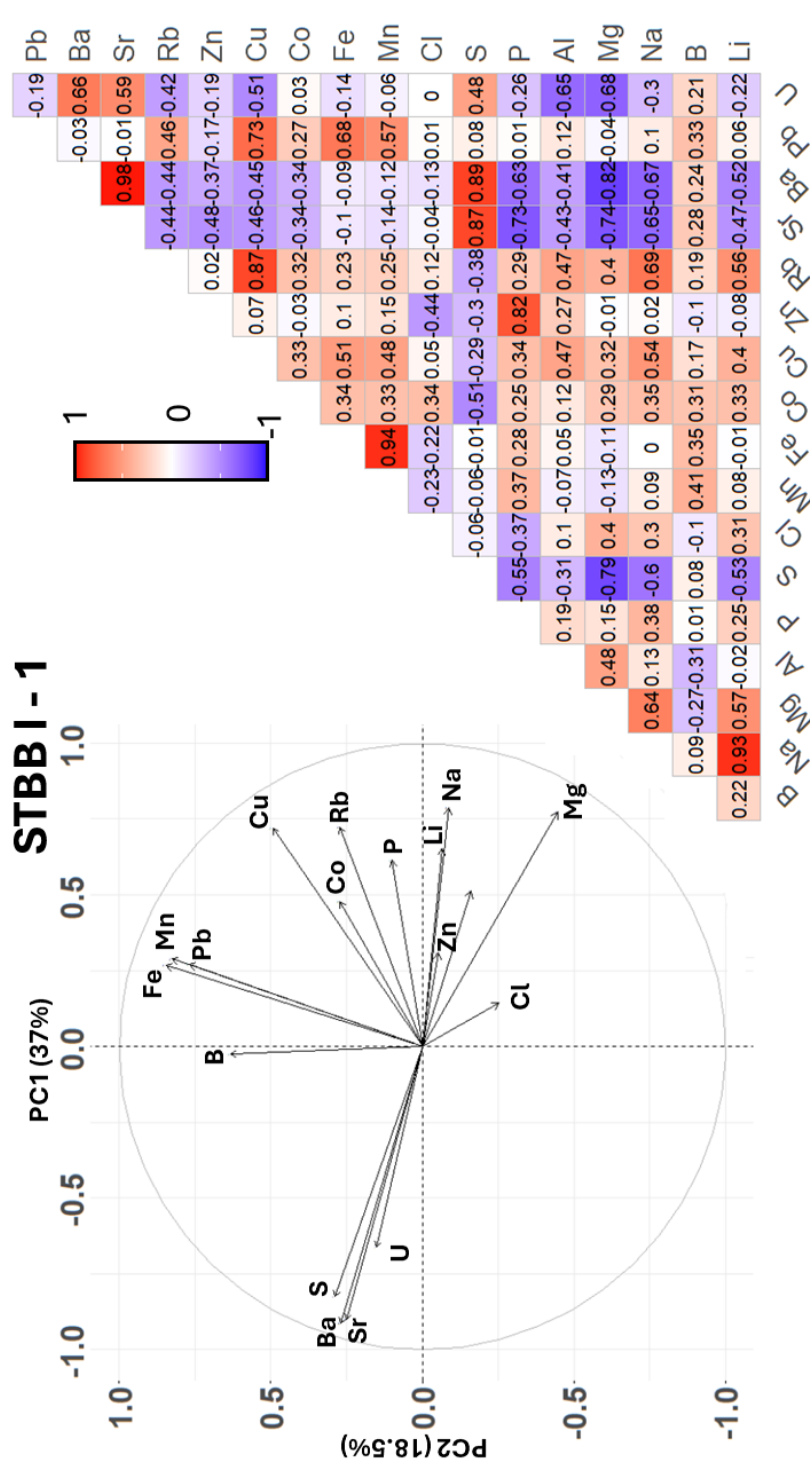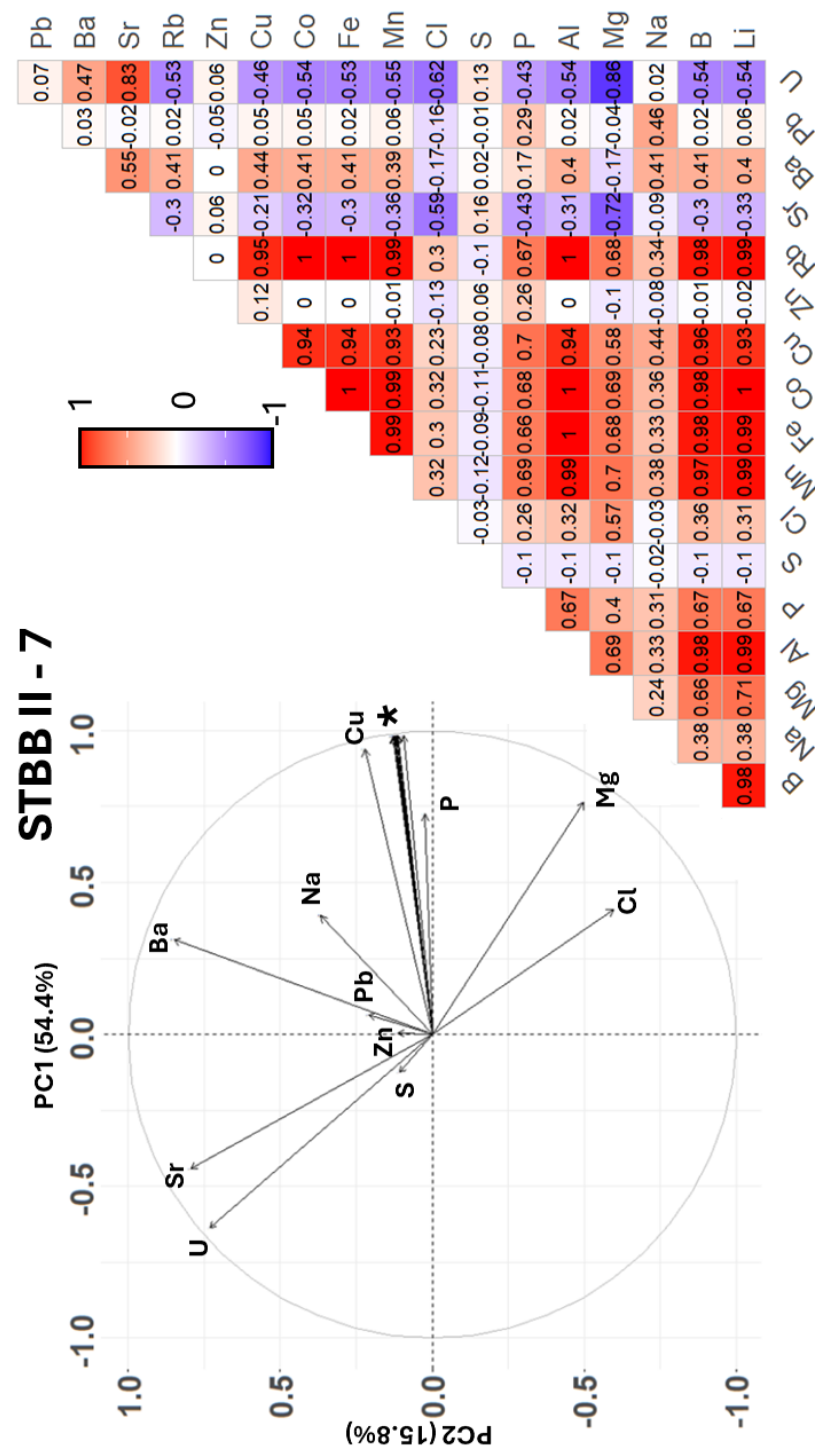
STBB I - 1

STBB II - 7

Figure S3S4: PCA plots (left) and correlation matrices (right) for trace element records in STBB I – 1 and STBB II - 7 (* denotes elements Al, B, Cu, Co, Fe, Li, Mn, and Rb).
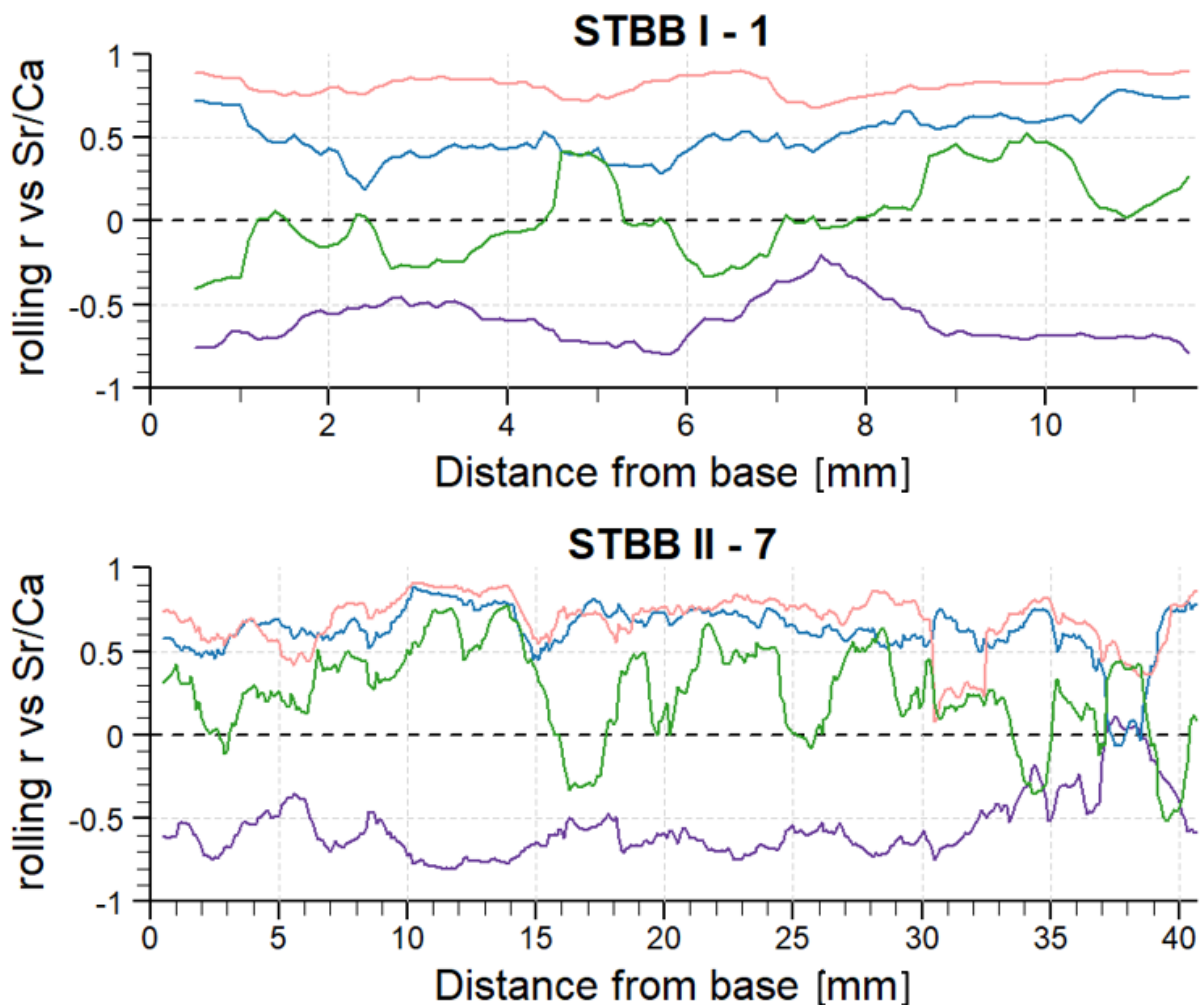
Figure S4S5: Trace element rolling Pearson's correlation coefficients vs Sr/Ca in STBB I – 1 and STBB II – 7 calculated over a 2 mm rolling window, at 0.1 mm intervals. Pink = Ba/Ca, Blue = U/Ca, Green = Mg/Ca, and purple = P/Ca. Ba/Ca and U/Ca show strong positive correlation along the entire length of both records, indicating a common PCP response. Phosphorus is anticorrelated in both records, peaking during high infiltration/low PCP episodes, when Sr/Ca declines. Mg/Ca fluctuates between periods of high and no correlation which we attribute to variable input of different dolomitic endmembers into dripwaters over the course of the record.

110
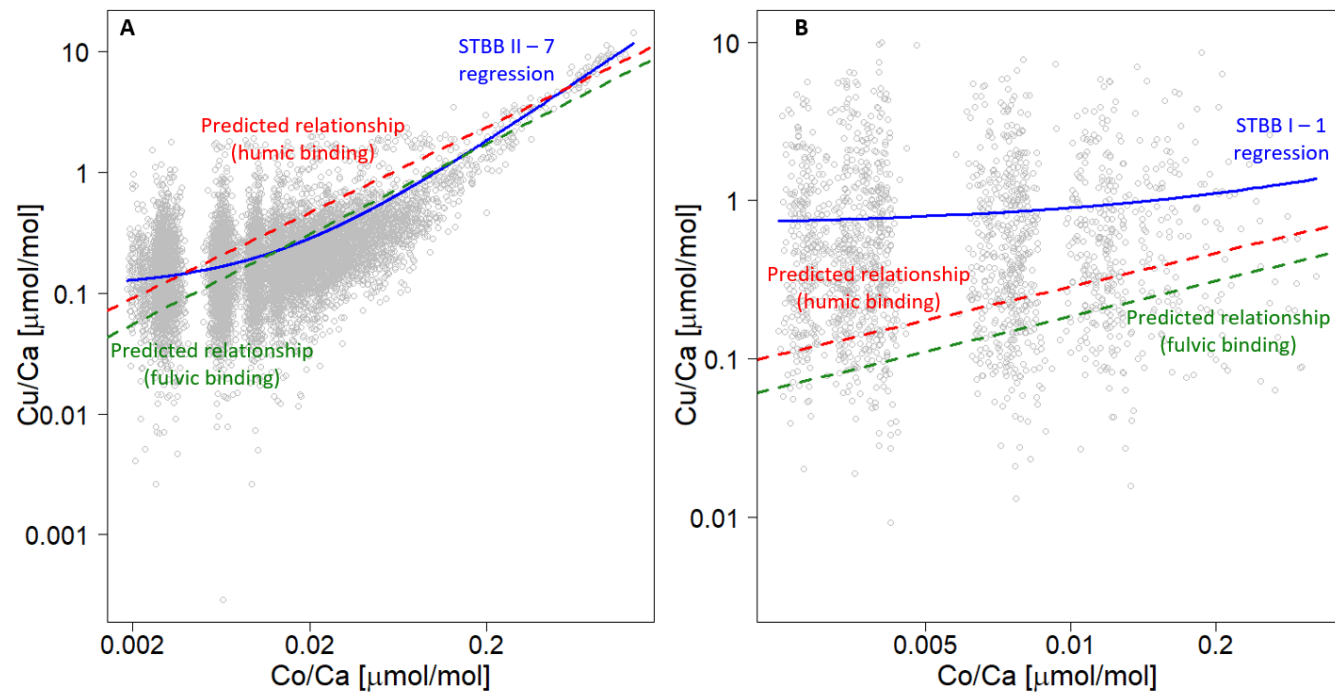
Figure S5S6: Cu vs Co concentrations in (A) STBB II – 7 and (B) STBB I – 1. Linear regressions (blue lines) pass through measured values (grey data points). Predicted metal ratios are drawn based on the equivalent n1 NICA Donnan humic ratios (red dotted lines, Milne et al. (2003) and fulvic binding affinity ratios (green dotted lines). STBB II – 7 measured values show greater agreement with
115 predicted values than STBB I – 1, reflecting the increased influence of organic binding in STBB II – 7 compared with STBB I – 1.

120

125

Figure S7: Comparison of z-score normalised Sr/Ca and grey values along a subsection of the STBB II – 7 where annual banding is observed. Annual bands are identified by maxima in grey value and align with peaks in Sr/Ca (a small offset between the records is likely given difficulty with visual alignment). Between 16 and 17 peaks are identified in the 3 mm transect, giving an average cycle period between 180 – 190 μm – confirming the seasonal ca. 0.2 mm derived through spectral analysis of the STBB II – 7 trace element records.

Comparison of Tortonian with modern hydrological regime methodology

140   We compared Miocene and modern-day hydrological seasonality using a 20-year instrumental record of precipitation from the nearby Samoylov Island Research Station (Boike et al., 2019). The proposed comparison method is based on time series analysis techniques and only offers a first estimate on how Miocene and recent seasonal precipitation predictability compare.

We employed dynamic time warping (DTW) (Berndt & Clifford, 1994), to align the Taba Bastaakh proxy records with the
145   instrumental precipitation and selected Sr/Ca, Ba/Ca, U/Ca, Mg/Ca and P/Ca as hydrological proxies for the evaluation of seasonality. Proxy records were detrended using Singular Spectrum Analysis (n = 500 samples) to ensure statistical estimates were not obscured by long-term variability (Vautard & Ghil, 1989). We pruned outliers based on peak detection, before averaging all five records to obtain a single mean record (the proxy stack-average - PSA). Spectral analysis reveals the most prominent peak at ~200 µm for the PSAs of both STBB II – 7 and STBB I – 1. This peak is also identified for most single
150   proxy records (Fig. S6). Hence, we assume this cycle to represent seasonal variability.

We downsampled the instrumental record by a moving average such that it exhibited the same number of samples per cycle as the speleothem PSA. We averaged seasonal cycles in the instrumental record to obtain a single mean cycle. This mean cycle was normalised to the same range as the respective PSA and repeated n_y times with the number of years n_y of each record,
155   yielding a template time series representative of typical modern seasonality. Each PSA was warped with the modern template time series. The DTW procedure returns an optimally adjusted (pseudo-)seasonal time axis for each stalagmite record (Fig. S8). It is important to stress that DTW solely stretches and squeezes the measured (mean) proxy values but does not introduce new values. This stretching and squeezing systematically minimises the Euclidean distance between the modern mean cycle and the record's (potentially) seasonal component. It projects the record's values onto a sub-annually resolved time axis that
160   can be anchored with a measured age. DTW can yield ties, i.e., suggest assigning several proxy values to the same time instance or assigning a single proxy value to several time instances. For the former case, we instead assign the proxy values to time instances in between the previous and the next time instances. For the latter case, we set the single proxy value to the centre of the suggested time instances. In this way, every proxy value and time instance only occurs once. The applied procedure can be regarded as a heuristic seasonal age model, returning a floating chronology with a relative time axis that helps to avoid
165   erroneous attribution of shifts that arise from variable speleothem growth rate (Braun et al., 2022, 2023). The analysis was carried out separately for both stalagmites.

Seasonality is evaluated by means of a simple power spectral measure: we compute the power spectral density of the modern as well as both PSA by means of Lomb-Scargle periodograms (Nyquist factor $n_{nyq} = 1$, no oversampling). Precipitation
170   seasonality is quantified by the total spectral power $|P|_s$ summed over the spectral band that closely encapsulates the seasonal peak (Fig. S9). The higher the power contained in the seasonal band, the more pronounced/stable the seasonal component in

the signal. Due to spectral leakage, seasonal spectral power manifests in a peak of finite width, i.e., seasonal power is distributed around this peak. We account for the respective uncertainty by varying the width of the spectral band between 0.2 (0.9 - 1.1) and 0.5 (0.75 - 1.25) (Fig. 6). We conclude that Tortonian seasonality was more pronounced compared to modern seasonality. In order to test the validity of our findings, we perform two crude numerical experiments: firstly, we modulate the modern seasonal record by a phase-matched sinusoidal. We increase the strength of the sinusoidal until the resulting seasonality $|P|_s$ matches the level observed for the Miocene. Conversely, we corrupt the PSAs with Gaussian white noise ($n = 1000$ realizations) of increasing intensity to examine how much noise is needed to reach the reduced modern level of seasonality. We conclude that modern seasonality would need to be amplified by a sinusoidal with 2.44x its magnitude to match Tortonian seasonality (averaged over both records), whereas Tortonian seasonality can be reduced to the modern value by corruption with 98% and 113 % white noise for STBB I – 1 and STBB II – 7 respectively (by means of its standard deviation). In this sense, and accounting for the considered uncertainties, the observed shift is deemed significant. However, we stress that due to their distinct mechanistic origin, a direct comparison between proxy and modern records presents more challenges that are not addressed by the performed procedure. An adequate transfer between proxy and precipitation variability would require proxy system modelling techniques and is beyond the scope of this study.
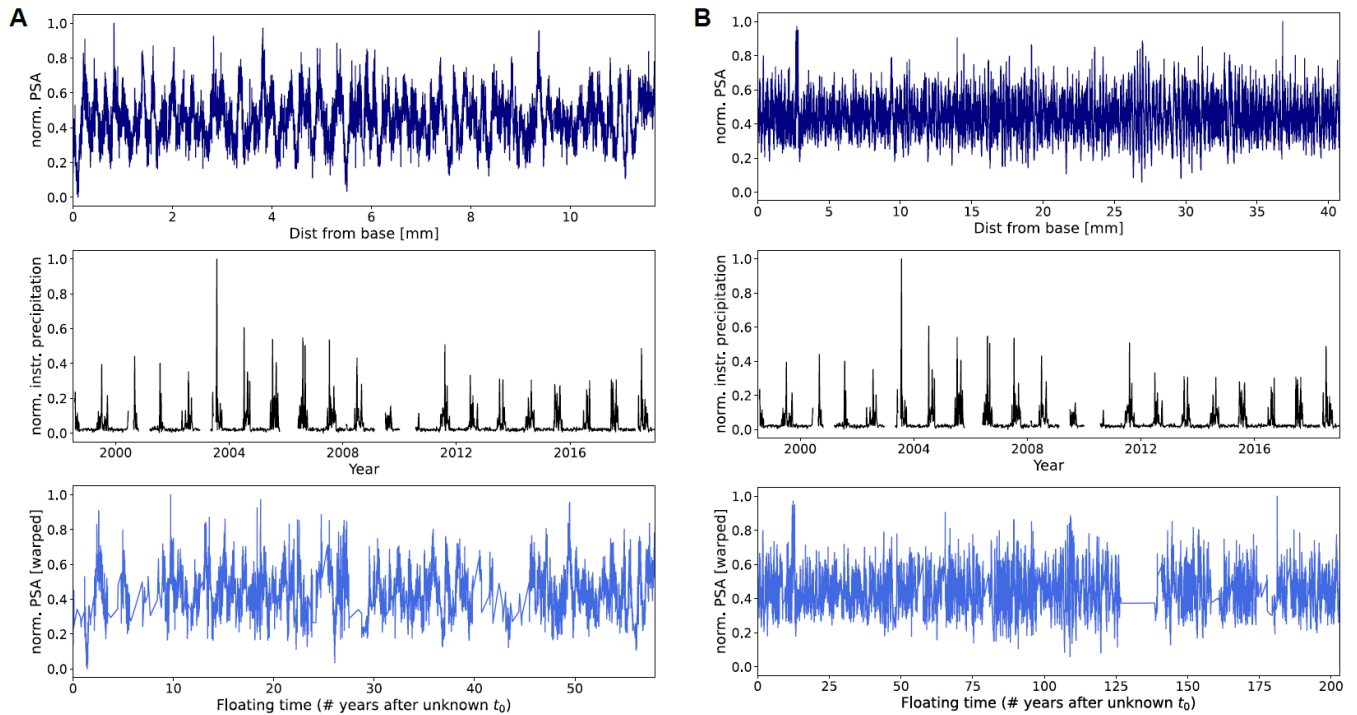
Figure S8: Results of dynamic time warping to align stacked proxy records for STBB I – 1 (A) and STBB II – 7 (B). Original detrended proxy stacks (dark blue), instrumental record of precipitation from the nearby Samoylov Island Research Centre (black), and warped proxy stacks (light blue).
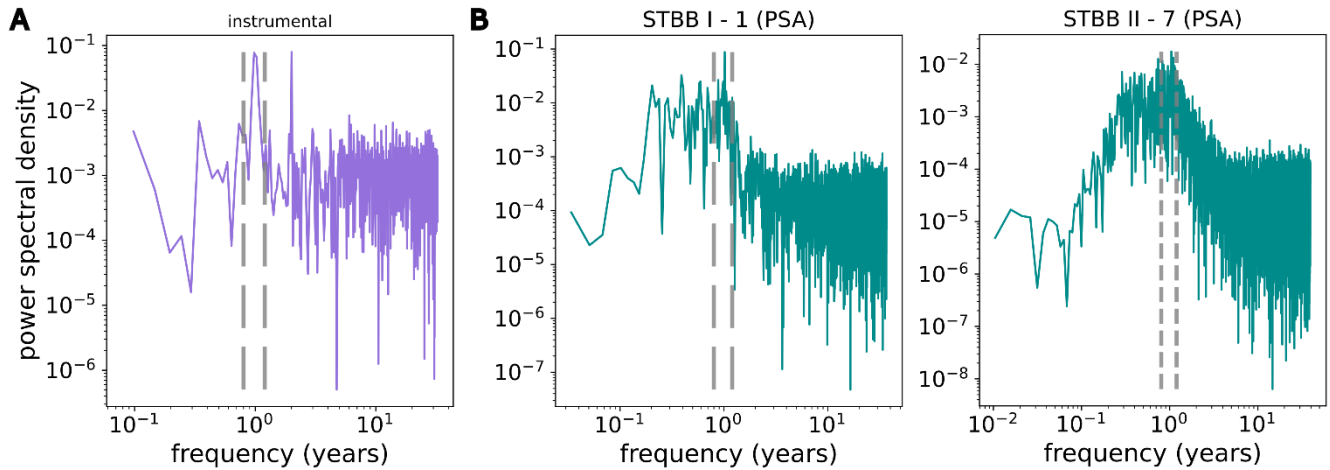
Figure S9: Lomb-Scargle periodograms of A), the 20-year instrumental record of precipitation from the nearby Samoylov Island and B), PSAs of both Taba Bastaakh proxy records. The seasonal measure employed here is defined as the total spectral power within the annual band (grey dashed lines).

References

Affek, H. P., Bar-Matthews, M., Ayalon, A., Matthews, A., and Eiler, J. M.: Glacial/interglacial temperature variations in Soreq cave speleothems as recorded by "clumped isotope" thermometry, Geochim Cosmochim Acta, 72, 5351–5360, https://doi.org/10.1016/j.gca.2008.06.031, 2008.

Berndt, D. J. and Clifford, J.: Using dynamic time warping to find patterns in time series, Proceedings of the 3rd international conference on knowledge discovery and data mining, 359–370, 1994.

Boike, J., Nitzbon, J., Anders, K., Grigoriev, M. N., Bolshiyanov, D. Y., Langer, M., Lange, S., Bornemann, N., Morgenstern, A., Schreiber, P., Wille, C., Chadburn, S., Gouttevin, I., and Kutzbach, L.: Measurements in soil and air at Samoylov Station (2002-2018), version 201908., Alfred Wegener Institute, 2019.

Braun, T., Fernandez, C. N., Eroglu, D., Hartland, A., Breitenbach, S. F. M., and Marwan, N.: Sampling rate-corrected analysis of irregularly sampled time series, Phys. Rev. E, 105, https://doi.org/10.1103/PhysRevE.105.024206, 2022.

Braun, T., Breitenbach, S. F. M., Skiba, V., Lechleitner, F. A., Ray, E. E., Baldini, L. M., Polyak, V. J., Baldini, J. U. L., Kennett, D. J., Prufer, K. M., and Marwan, N.: Decline in seasonal predictability potentially destabilized Classic Maya societies, Commun Earth Environ, 4, 82, https://doi.org/10.1038/s43247-023-00717-5, 2023.

Craig, H.: Isotopic variations in meteoric waters, Science (1979), 133, 1702–1703, https://doi.org/10.1126/science.133.3465.1702, 1961.

Daëron, M., Guo, W., Eiler, J., Genty, D., Blamart, D., Boch, R., Drysdale, R., Maire, R., Wainer, K., and Zanchetta, G.: 13C18O clumping in speleothems: Observations from natural caves and precipitation experiments, Geochim Cosmochim Acta, 75, 3303–3317, https://doi.org/10.1016/j.gca.2010.10.032, 2011.

215 Gabitov, R. I., Watson, E. B., and Sadekov, A.: Oxygen isotope fractionation between calcite and fluid as a function of growth rate and temperature: An in-situ study, Chem Geol, 306–307, 92–102, https://doi.org/10.1016/j.chemgeo.2012.02.021, 2012.

Kele, Breitenbach, Sebastian, Capezzuoli, Meckler, Ziegler, Millan, Kluge, Hanselmann, John, Yan, Liu, and Bernasconi: Temperature dependence of oxygen- and clumped isotope fractionation in carbonates: A study of travertines and tufas in the 6-95 C temperature range, Geochim Cosmochim Acta, 168, 172–192, https://doi.org/10.1016/j.gca.2015.06.032, 2015.

220 Kluge, T. and Affek, H. P.: Quantifying kinetic fractionation in Bunker Cave speleothems using Δ 47, Quat Sci Rev, 49, 82–94, https://doi.org/10.1016/j.quascirev.2012.06.013, 2012.

Meckler, A. N., Vonhof, H., and Martínez-García, A.: Temperature reconstructions using speleothems, Elements, 17, 101–106, https://doi.org/10.2138/GSELEMENTS.17.2.101, 2021.

Milne, C. J., Kinniburgh, D. G., Van Riemsdijk, W. H., and Tipping, E.: Generic NICA - Donnan model parameters for metal-225 ion binding by humic substances, Environ Sci Technol, 37, 958–971, https://doi.org/10.1021/es0258879, 2003.

Spors, S.: Stable Water Isotope Characteristics of Recent Precipitation from Tiksi and Samoylov Island-Calibration of a Geoscientific Proxy for Northern Siberia: Bachelors Thesis, Institut für Erd- und Umweltwissenschaften, Universität Potsdam, Potsdam, 2018.

Tripati, A. K., Hill, P. S., Eagle, R. A., Mosenfelder, J. L., Tang, J., Schauble, E. A., Eiler, J. M., Zeebe, R. E., Uchikawa, J., 230 Coplen, T. B., Ries, J. B., and Henry, D.: ScienceDirect Beyond temperature : Clumped isotope signatures in dissolved inorganic carbon species and the influence of solution chemistry on carbonate mineral composition, Geochim Cosmochim Acta, 166, 344–371, https://doi.org/10.1016/j.gca.2015.06.021, 2015.

Uemura, R., Kina, Y., Shen, C. C., and Omine, K.: Experimental evaluation of oxygen isotopic exchange between inclusion water and host calcite in speleothems, Climate of the Past, 16, 17–27, https://doi.org/10.5194/cp-16-17-2020, 2020.

235 Vautard, R. and Ghil, M.: Singular spectrum analysis in nonlinear dynamics, with applications to paleoclimatic time series, Physica D: Nonlinear Phenomena, 35, 395–424, 1989.

York, D., Evensen, N. M., Martínez, M. L., and De Basabe Delgado, J.: Unified equations for the slope, intercept, and standard errors of the best straight line, Am J Phys, 72, 367–375, https://doi.org/10.1119/1.1632486, 2004.